Preprints, 10th IFAC International Symposium on
Advances in Automotive Control
Columbus, Ohio, USA, August 28-30, 2022

Vehicle Model Predictive Trajectory Tracking Control with Curvature and Friction Preview

Liming Gao*. Craig Beal. Juliette Mitrovich*. Sean Brennan***

** The Pennsylvania State University, University Park, PA 16802 USA (e-mail: lug358@psu.edu; jfm5876@psu.edu; snb10@psu.edu).*

*** Bucknell University, Lewisburg, PA17837 USA (e-mail:cbeal@bucknell.edu)*

Abstract: Autonomous vehicle trajectory tracking control is challenged by situations of varying road surface friction, especially in the scenario where there is a sudden decrease in friction in an area with high road curvature. If the situation is unknown to the control law, vehicles with high speed are more likely to lose tracking performance and/or stability, resulting in loss of control or the vehicle departing the lane unexpectedly. However, with connectivity either to other vehicles, infrastructure, or cloud services, vehicles may have access to upcoming roadway information, particularly the friction and curvature in the road path ahead. This paper introduces a model-based predictive trajectory-tracking control structure using the previewed knowledge of path curvature and road friction. In the structure, path following and vehicle stabilization are incorporated through a model predictive controller. Meanwhile, long-range vehicle speed planning and tracking control are integrated to ensure the vehicle can slow down appropriately before encountering hazardous road conditions. This approach has two major advantages. First, the prior knowledge of the desired path is explicitly incorporated into the computation of control inputs. Second, the combined transmission of longitudinal and lateral tire forces is considered in the controller to avoid violation of tire force limits while keeping performance and stability guarantees. The efficacy of the algorithm is demonstrated through an application case where a vehicle navigates a sharply curving road with varying friction conditions, with results showing that the controller can drive a vehicle up to the handling limits and track the desired trajectory accurately.

Keywords: Autonomous vehicles, friction preview, model predictive control, path tracking control, vehicle control, vehicle dynamics.

1. INTRODUCTION

Path tracking control is one of the most challenging tasks of autonomous vehicles, especially when maneuvering in hazardous road conditions such as snow, ice, rain, etc. (Bithar, 2020; Litman, 2022). Vehicles with high speeds are more likely to run off the road or lose control unexpectedly when encountering a road segment with an unforeseen sudden decrease in friction while in an area with high road curvature.

Much research has been conducted to address the challenging tracking problem in hazardous conditions based on model predictive control (MPC). MPC can predict and optimize vehicle dynamics states in the future based on a planned control command sequence. This has the advantage of dealing with multiple control objectives respecting state and input constraints, while explicitly incorporating vehicle stabilization into path tracking. For example, Falcone *et al* and Katriniok *et al* presented MPC controllers to track the lane change trajectory on a slippery road while limiting the tire force in the desired force regime (Falcone et al., 2007; Katriniok et al., 2013).

While these approaches directly incorporate vehicle stabilization into path tracking, they still suffer from the underlying challenge that tracking a curvy path with extremely high speed or sudden decrease of road friction could result in a large tracking error and/or loss of stability. In this situation, tire forces are limited and thus a controller must prioritize some combination of path tracking or stability goals, but not both completely. This limitation suggests frameworks that combine MPC trajectory tracking algorithms with a speed planning algorithm to offer a complete guidance controller. Funke *et al* (Funke et al., 2017) proposed such a decoupled framework where a simple controller computes the vehicle longitudinal force to track an off-line planned speed profile; then, an MPC determines the lateral inputs for path tracking and stabilization. Similarly, Ni *et al* (Ni et al., 2017) used three sub-controllers to conduct the speed tracking, vehicle stabilization, and path following respectively. In these controllers, the decoupled speed planning and longitudinal controller enable the vehicle to slow down prior to tight curvature change. This mitigates the need for the vehicle to react as aggressively during the onset of instability or path departure because, when operating with lower velocities, vehicles generally have a larger stable operating region and can reserve tire forces to follow the desired path (Beal & Gerdes, 2013; Cao et al., 2017).

However, the aforementioned approaches assume a known and/or constant friction, or an instantaneous measurement of friction. If this assumption is violated, then controller

performance or stability guarantees are also violated. However, with connectivity either to other vehicles, infrastructure, or cloud services, vehicles may have access to upcoming roadway information, particularly the friction and curvature in the road path ahead (Gao et al., 2021; Panahandeh et al., 2017). This type of foreknowledge could allow a vehicle path tracking control system to work more reliably and proactively.

This paper introduces a trajectory tracking controller structure that integrates speed planning and tracking, path following, and vehicle stabilization using previewed knowledge of path curvature and road friction. In the structure, an explicit speed profile is planned first according to the vehicle dynamic limits using a long-range preview of path curvature and friction obtained from a cloud database. Next, a longitudinal controller calculates the desired total traction or braking force to track the speed profile, allowing for some user-defined maneuvering margin. A short-range path prediction of curvature, friction, and longitudinal commands from the longitudinal controller is then used by an MPC controller to determine the immediate lateral inputs for path following and stabilization.

There are two major advantages of this approach. First, the preview of the desired path is explicitly incorporated into the computation of control inputs. Second, the combination of longitudinal and lateral tire forces is considered in the control approach to avoid violation of tire force limits while keeping performance and stability guarantees. Consecutively, Section II introduces path description and the vehicle dynamics model used in the speed planning and stability envelopes outlined in Section III. Section IV details the proposed controller structure which is verified through numerical simulation experiments discussed in Section V. Finally, the conclusion and future work are given in Section VI.

2. PATH AND VEHICLE MODEL DESCRIPTION

2.1 Path description

The term "path" in this work denotes the desired route the vehicle aims to follow. It is assumed to be known and is parameterized by curvature κ and friction coefficient μ as a function of station s which is the distance measured along the path. Friction is assumed to be uniform in the lateral direction of the path but can change suddenly in the station direction, e.g., the direction of travel. The path example used in this work is shown in Fig. 1 and is designed as a challenging driving scenario in which a low friction region suddenly occurs in the path segment with high curvature.

2.2 Vehicle model

The single-track planar "bicycle model", shown in Fig. 2, is used to represent the vehicle with the small-angle assumption. For a given longitudinal velocity U_x, the vehicle lateral velocity U_y and yaw rate r states are governed by:

$$\begin{aligned} \dot{U}_y &= \frac{F_{yf}+F_{yr}}{m} - rU_x \\ \dot{r} &= \frac{aF_{yf}-bF_{yr}}{I_{zz}} \end{aligned}, \qquad (1)$$

where F_{yf} and F_{yr} are the lateral forces acting on the front and rear tires, respectively. The vehicle parameters include the

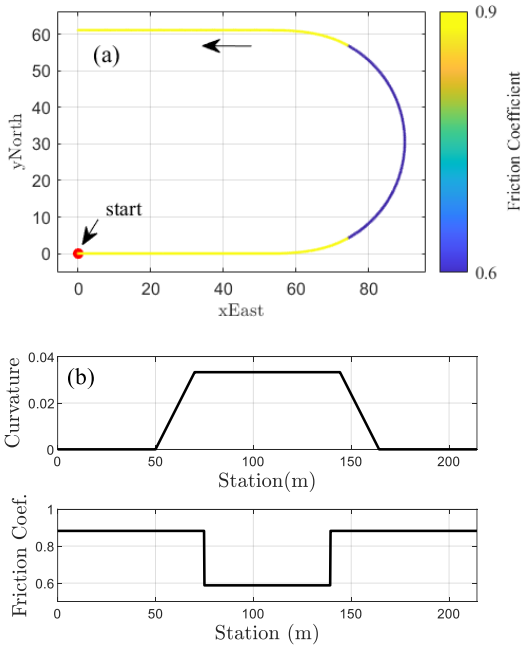

Figure 1. Sample path: (a) path shape; (b) path curvature and friction coefficient.

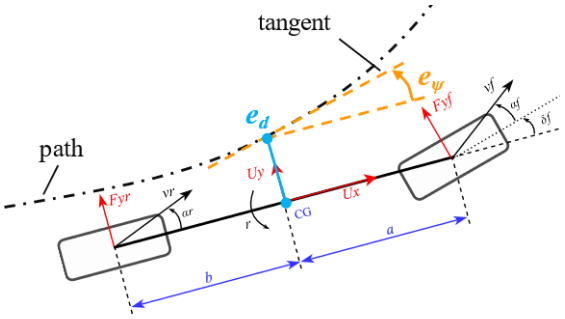

Figure 2. Planar single-track vehicle chassis model with front steering.

vehicle mass m, yaw moment of inertia I_{zz}, the distances from the vehicle's center of gravity to the front and rear axle a and b, respectively.

Tire force F_{yf} and F_{yr} in (1) are defined by the nonlinear "brush" tire model (Pacejka, 2012):

$$\begin{aligned} F_y &= \begin{cases} C_\alpha \tan\alpha + \dfrac{C_\alpha^2}{3\mu\rho F_z}|\tan\alpha|\tan\alpha \\ \quad + \dfrac{C_\alpha^3}{27\mu^2\rho^2 F_z^2}\tan^3\alpha & ,|\alpha| \le \alpha_{peak} \\ -\mathrm{sgn}(\alpha)\mu\rho F_z = -\mathrm{sgn}(\alpha)F_{y,\max} & ,\text{otherwise} \end{cases} \\ &= f_{tire}(\mu,\alpha,F_x) \end{aligned} \qquad (2)$$

where μ is the road-tire friction coefficient, C_α is the tire cornering stiffness, and F_z is the tire normal load. α is the tire sideslip angle, and $\alpha_{peak} = \tan^{-1}(3\mu\rho F_z/C_\alpha)$ is the peak sideslip angle. In this paper, the forces F_z at tires are assumed to be constant. Note: ρ is a factor to capture the reduced lateral force due to tire longitudinal force F_x. The factor is defined based on friction circle constraints but could also be used, as extensions

of this work, to account for load transfer (Brach & Brach, 2011):

$$\rho = \sqrt{(\mu F_z)^2 - F_x^2} \,/\, \mu F_z \,. \tag{3}$$

To obtain a linear model useful for MPC controller design, the tire sideslip angles in the front (α_f) and rear (α_r) are described linearly in terms of the vehicle states and the steering angle input with the small-angle assumption:

$$\alpha_f = \frac{U_y + ar}{U_x} - \delta_f, \alpha_r = \frac{U_y - br}{U_x}, \tag{4}$$

where δ_f is the front steering angle.

The input to the vehicle model (1) is front lateral force F_{yf}, which can be mapped into steering angle δ_f using (4):

$$\delta_f = \frac{U_y + ar}{U_x} - \alpha_{f,d}\,, \tag{5}$$

where $\alpha_{f,d}$ is the desired tire sideslip angle, which can be calculated through the inverse model of (2) f_{tire}^{-1} . f_{tire}^{-1} has a closed-form solution:

$$\begin{aligned} \alpha_{f,d} &= f_{tire}^{-1}\left(F_{yf}, \mu, F_x\right) \\ &= \tan^{-1}\left(3F_{yf}\left(\mu\rho\,\mathrm{sgn}(F_{yf}) + \sqrt[3]{\mu^2\rho^2(1-\mu\rho\,\mathrm{sgn}(F_{yf}))}\right)\Big/ C_{\alpha f}\right) \end{aligned} \tag{6}$$

when $\alpha_{f,d}$ does not exceed the angle corresponding to tire peak force, i.e. $|\alpha_{f,d}| \le \alpha_{f,d,peak}$. This tire sideslip angle operation condition is assumed for the use of this equation. Using F_{yf} as the model input, rather than steering angle, still results in a linear vehicle model and allows for the controller to explicitly account for the force capability of the front steering tire.

However, this approach is not applicable for the rear tire due to the lack of rear steering actuation. Alternatively, the brush model of rear tire lateral force F_{yr} is linearized at a nominal operation point $(\bar{\mu}, \bar{\alpha}_r, \bar{F}_x)$ as an affine function of α_r:

$$F_{yr} = \bar{F}_{yr} + \bar{C}(\alpha_r - \bar{\alpha}_r)\,, \tag{7}$$

where $\overline{F_{yr}}$ and $\bar{C}$ are lateral tire force and equivalent cornering stiffness at the nominal point. This linearization preserves the model convexity and represents the nonlinear tire behavior near the nominal point (Beal & Gerdes, 2013). When used in the model predictive controller, the linearization equation (7) is conducted for successive nominal points in the prediction horizon. The successive sequence of $\bar{\mu}$ is obtained through the prior knowledge of the desired path and $\overline{F_x}$ is provided by the longitudinal controller which is detailed in section 4.1. The sequence of $\bar{\alpha}_r$ is approximated based on the last step vehicle states predicted by the controller because its exact values are not known a priori. This successive linearization is necessary, as the friction and F_x may change significantly in the prediction horizon in this work. Thereby, linearizing the tire force in the whole prediction horizon with the nominal point in the initial time step of the prediction horizon (Beal & Gerdes, 2013) may not be reasonable.

The path following states, including heading error between the vehicle and path e_ψ and lateral deviation from path e_d, are modeled as:

$$\begin{aligned} \dot{e}_\psi &= r - U_x\kappa(s) \\ \dot{e}_d &= U_y + U_x e_\psi \end{aligned}\,. \tag{8}$$

Combining (1), (7) and (8), a time-varying affine force input (AFI) model can be obtained governing vehicle lateral dynamics and path tracking kinematics, namely the so-called "bicycle model" which is now linear if constant longitudinal velocity is assumed. This is expressed as:

$$\begin{aligned} \dot{x}(t) &= A(t)x(t) + B_F F_{yf}(t) + B_\kappa(t)\kappa(t) + d(t) \\ y(t) &= Cx(t) \end{aligned}\,, \tag{9}$$

with

$$x(t) = \begin{bmatrix} U_y & r & e_\psi & e_d \end{bmatrix}^T,$$

$$A(t) = \begin{bmatrix} \dfrac{\bar{C}_{\bar{\alpha}_r}(t)}{mU_x(t)} & -\dfrac{b\bar{C}_{\bar{\alpha}_r}(t)}{mU_x(t)} - U_x(t) & 0 & 0 \\ \dfrac{-b\bar{C}_{\bar{\alpha}_r}(t)}{I_z U_x(t)} & \dfrac{b^2\bar{C}_{\bar{\alpha}_r}(t)}{I_z U_x(t)} & 0 & 0 \\ 0 & 1 & 0 & 0 \\ 1 & 0 & U_x(t) & 0 \end{bmatrix},$$

$$B_F = \begin{bmatrix} \dfrac{1}{m} & \dfrac{a}{I_z} & 0 & 0 \end{bmatrix}^T,\; B_K(t) = \begin{bmatrix} 0 & 0 & -U_x(t) & 0 \end{bmatrix}^T,$$

$$d(t) = \begin{bmatrix} \dfrac{(\bar{F}_{yr}(t) - \bar{C}_{\bar{\alpha}_r}(t)\bar{\alpha}_r(t))}{m} & \dfrac{-b(\bar{F}_{yr}(t) - \bar{C}_{\bar{\alpha}_r}(t)\bar{\alpha}_r(t))}{I_z} & 0 & 0 \end{bmatrix}^T.$$

The output states are path tracking errors with

$$C = \begin{bmatrix} 0 & 0 & 1 & 0 \\ 0 & 0 & 0 & 1 \end{bmatrix}.$$

Note that $A(t)$, $B_\kappa(t)$, and $d(t)$ depend on F_x, U_x, and $\bar{\alpha}_r$. The nonlinearity of tire forces is incorporated in the affine model (9) in a convex way. The model can be discretized for linear MPC implementation.

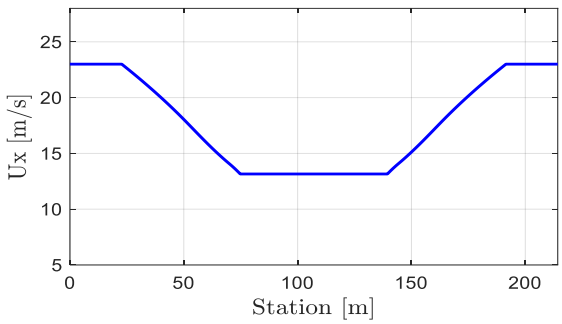

Figure 3. Generated speed profile with previewed path curvature and friction.

3. SPEED PROFILE AND STABILITY ENVELOPE

3.1 Speed profile planning

The speed profile defines the desired vehicle longitudinal velocity $U_{x,d}(s)$ at each station point s along the path. With the previous work (Gao et al., 2021), the longitudinal speed governing equation based on the road-tire force limit is:

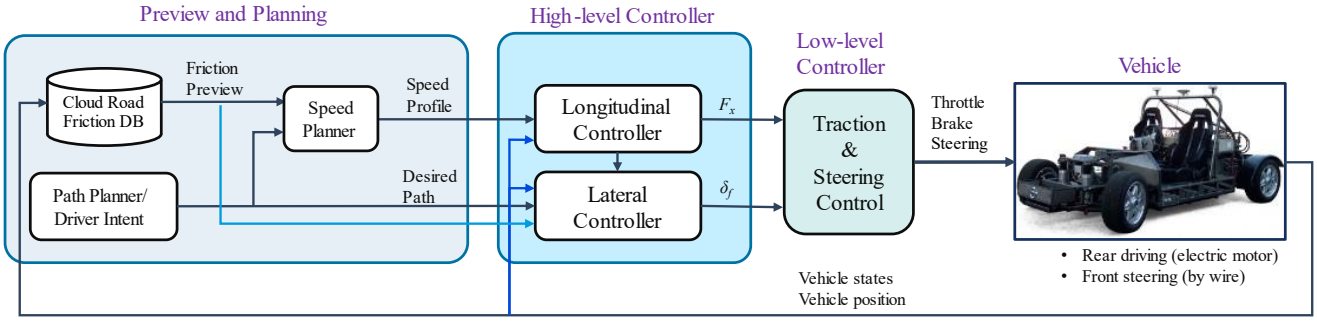

Figure 4. Control structure: the high-level controller calculates the longitudinal and then lateral inputs for the vehicle.

$$\frac{dU_{x,d}(s)}{ds}=\frac{1}{U_{x,d}(s)}\left(\pm\frac{a}{L}\sqrt{\left(\mu_{des}(s)g\right)^2-\left(\kappa(s)U_{x,d}^2(s)\right)^2}\right), \quad (10)$$

where $L = a+b$ and g is the gravitational acceleration. This equation yields closed-form solutions under common road conditions or can be solved numerically. Applying (10) to the previewed path curvature $\kappa(s)$ and friction coefficient $\mu(s)$ shown in Fig. 1 and setting the design friction term to give a small margin relative to the friction limit, $\mu_{des}(s) = 0.95\mu(s)$, the speed profile near the vehicle handling limits can be calculated. The result is shown in Fig. 3.

3.2 Stability Envelope

The controller in this work uses the stability envelope formulation suggested by Beal and Gerdes (Beal & Gerdes, 2013), which bounds the vehicle lateral states U_y and r by the maximum available tire force. The envelope constraints can be expressed as a time-varying linear inequality:

$$\left|E_{\lim}(t)x(t)\right|\le G_{\lim}(t)\,, \quad (11)$$

where

$$E_{\lim}(t)=\begin{bmatrix}0 & 1 & 0 & 0\\ 1/U_x(t) & -b/U_x(t) & 0 & 0\end{bmatrix} \quad (12)$$

$$G_{\lim}(t)=\begin{bmatrix}r_{\lim}(t)\\ \alpha_{r,\lim}(t)\end{bmatrix}=\begin{bmatrix}\min\left(\dfrac{(1+b/a)F(t)_{yr,\max}}{mU_x(t)},\dfrac{(1+a/b)F(t)_{yf,\max}}{mU_x(t)}\right)\\ \arctan(\dfrac{3\mu(t)}{C_{\alpha r}}\dfrac{amg}{L})\end{bmatrix}. \quad (13)$$

Vehicle stability is guaranteed for all states residing in the envelope. Leaving this boundary does not necessarily lead to instability, but the control action which can move the vehicle states monotonically back to the envelope boundaries in the next time step may not exist. Equation (11) reveals that a vehicle has a larger stable operating region with a smaller speed U_x, which implies the necessity of speed planning and control for path following in hazardous road conditions.

4. CONTROL STRUCTURE

The overall trajectory tracking control structure proposed in this paper is illustrated in Fig. 4. In the structure, the first step is to obtain the long-range preview of path curvature and friction from a cloud friction database. With the preview, an explicit speed profile can be calculated using the method in section 3.1. Next, a longitudinal controller calculates the desired total traction force to track the speed profile. A short-range preview of path curvature, path friction, and longitudinal commands from the longitudinal controller is then used by an MPC controller to determine the immediate steering angle for path following and stabilization. Thereby, the trajectory tracking problem is decomposed into a longitudinal speed planning and tracking, and a lateral path following problem.

4.1 Longitudinal controller

As the first step, a feedforward-feedback longitudinal controller calculates desired longitudinal forces at each point k in the prediction horizon to track the speed profile:

$$F_{xd,k}=ma_{x,d}(s_k)+K_v(U_{x,d}(s_k)-U_{x,k})\,, \quad (14)$$

where $U_{x,d}(s_k)$ and $a_{x,d}(s_k)$ are the desired speed and acceleration from the planned speed profile at station s_k, and K_v is a speed tracking error gain. The longitudinal states in the optimization horizon are provided to the lateral controller to solve for the lateral inputs.

4.3 Lateral controller

The MPC lateral controller solves for optimal front tire steering forces as the input with stability and model constraints to ensure path following and stability. The optimization problem is described as:

$$\min \sum_{k=0}^{N}\left(y_k-y_{d,k}\right)^T Q_k\left(y_k-y_{d,k}\right)+\sum_{k=0}^{N-1}F_{yf,k}^T R_k F_{yf,k}+\sum_{k=0}^{N}\left\|S_k\eta_k\right\|_1 \quad (15.1)$$

subject to

$$x_{k+1}=A_{d,k}x_k+B_{Fd,k}F_{yf,k}+B_{Kd,k}K_{path.k}+d_k, k=0,\ldots,N-1 \quad (15.2)$$
$$y_k=C_d x_k, k=0,\ldots,N$$

$$\left|F_{yf,k}\right|\le F_{yf,\max,k}, k=0,\ldots,N-1 \quad (15.3)$$

$$\left|F_{yf,k+1}-F_{yf,k}\right|\le F_{yf,slew,k}, k=0,\ldots,N-2 \quad (15.4)$$
$$\left|F_{yf,0}-F_{yf,\text{prev}}\right|\le F_{yf,slew,0}$$

$$\left|E_{\lim,k}x_k\right|\le G_{\lim,k}+\eta_k, k=0,\ldots,N \quad (15.5)$$

$$\eta_k\ge 0, k=0,\ldots,N\,. \quad (15.6)$$

Equation (15.1) represents the objective function, where the desired tracking states $y_{d,k}$ is generally set as zero. Equations

(15.2) - (15.4) describe the hard dynamic constraints that the solution must obey: Equation (15.2) is the discretized vehicle model of (9) using the Tustin method which has a closed-form solution, (15.3) restricts the maximum available lateral tire force which is estimated through previewed friction coefficient and the normal load on the front steering tire, and (15.4) restricts force slew rate which is limited by the capabilities of the steering actuator. The inequality (15.5) is used to restain the vehicle states within the stability envelope defined by (11). The positive slack variables defined by the final term (15.6) are added to soften the stability envelope boundaries to guarantee a feasible solution for the optimization problem. Q, R, and S are penalty weights that mediate the prioritization of each term in the objective function. Quadratic costs on output states error and input F_{yf} allow small deviations of these qualities but cause strong penalization for large deviations. The linear cost on the slack variable η penalizes small violations immediately. As is common with MPC, only the first step optimal input solution $F_{yf,0,opt}$ is applied to the vehicle, then the entire optimization is recalculated at the next time step. Note that the desired front lateral tire force can be converted into a steering angle using (5) and (6).

5. NUMERICAL SIMULATION

The performance of the proposed MPC-based trajectory controller was evaluated by a MATLAB/Simulink simulation where a dual-track nonlinear vehicle body and coupled brush tire models are employed as the simulation control plant. The given formulation causes the optimization problem (15) to be a convex quadratic program that can be exploited to produce an efficient solver for real-time implementation through CVXGEN (Mattingley & Boyd, 2012). The MPC parameters are shown in Table 1.

Table 1. Controller parameters and weights

Parameter	Symbol	Value	Units
MPC Prediction Horizon	Np	20	steps
MPC time step	Ts	0.05	second
Lateral error weight	Q_{ed}	300	1/m^2
Heading error weight	$Q_{e\psi}$	500	1/rad^2
Input force weight	R_{Fyf}	$1*10^{-7}$	1/N^2
Yaw rate slack weight	S_r	$1*10^{2}$	s/rad
Sideslip angle slack weight	S_α	$1*10^{2}$	1/rad
Input slew rate limit	$dF_{yf,max}$	1000	N/s

Simulation results test the controller in tracking the challenging path shown in Fig. 1 at speeds that maximize friction utilization up to 95%. Fig. 6 and Fig. 9 present the vehicle speed and tire forces to demonstrate the performance of the longitudinal controller. One can see that before encountering the region with low friction and high curvature, the vehicle starts to slow down by demanding maximum available tire forces. Then the vehicle keeps a constant speed in the low friction region. The proactive speed adjustment allows the vehicle to have a larger stable operating region and reserve tire forces to follow the desired path.

Fig. 5 presents the tracking errors. The maximum absolute lateral deviation error is less than 0.08 m which occurs when entering the low friction region. Fig. 7 indicates vehicle states are safely inside the varying stability boundaries. The variation reflects the changing of path friction and available tire forces. Fig. 9 depicts the actual tire forces are almost within the estimated limits. It can be observed that all the tire forces are commanded to provide the lateral cornering when the vehicle is tracking the low friction circular path at a constant speed. Examining Fig. 8, the steering is operating quickly to stabilize the vehicle and thereafter follow the path when the vehicle passes the transition edge between high and low friction regions. All the results show that the controller could drive the vehicle near the handling limits and track the desired trajectory accurately without loss of stability.

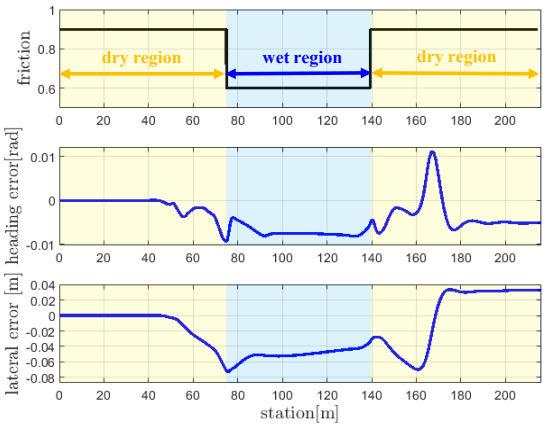

Figure 5. Trajectory tracking errors.

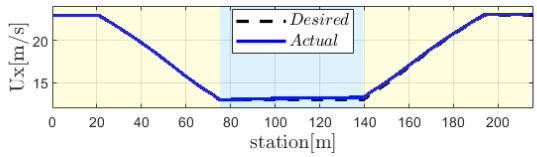

Figure 6. Vehicle speed.

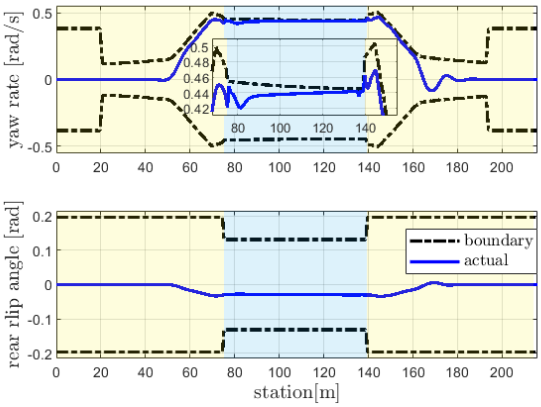

Figure 7. Trajectory tracking stability states.

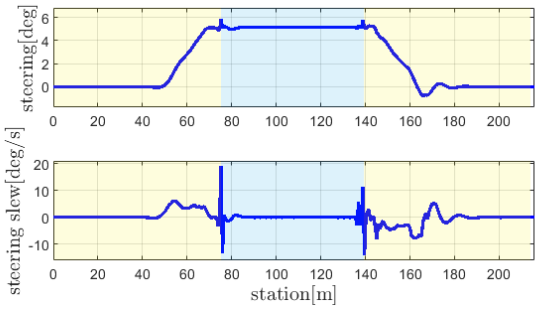

Figure 8. Steering inputs.

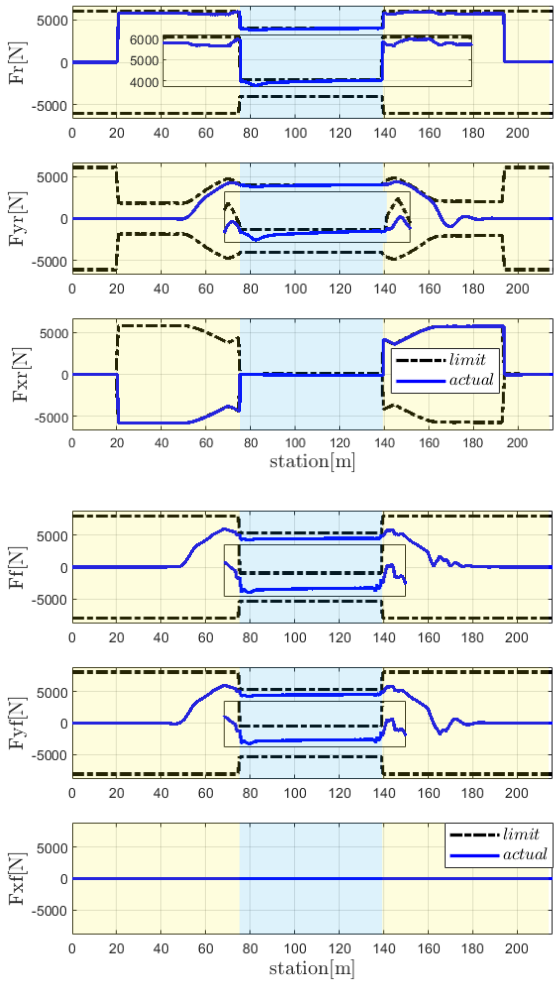

Figure 9. Tire forces: (a) rear tire; (b) front tire.

6. CONCLUSIONS AND FUTURE WORK

In this work, a longitudinal-lateral trajectory tracking control structure is presented, where path following and stabilization are incorporated through MPC. Meanwhile, long-range speed planning and tracking control are used to ensure the vehicle can slow down before encountering hazardous road conditions. In the future, the control framework can be readily extended to include not only the curvature and friction variations but also grade and bank, both of which are common features in real road scenarios. Additionally, the vehicle load transfer due to acceleration, which results in a non-constant normal force at each tire in a real vehicle, can be included in the vehicle model for speed planning and control. Finally, the convex formulation of MPC allows its real-time deployment in the future.

REFERENCES

Beal, C. E., & Gerdes, J. C. (2013). Model predictive control for vehicle stabilization at the limits of handling. *IEEE Transactions on Control Systems Technology*, *21*(4), 1258–1269. https://doi.org/10.1109/TCST.2012.2200826

Bithar, V. (2020). *Robust MPC based Motion Planning and Control of Autonomous Ground Vehicles*. The Ohio State University.

Brach, R., & Brach, M. (2011). The tire-force ellipse (Friction Ellipse) and tire characteristics. *SAE 2011 World Congress and Exhibition*. https://doi.org/10.4271/2011-01-0094

Cao, H., Song, X., Zhao, S., Bao, S., & Huang, Z. (2017). An optimal model-based trajectory following architecture synthesising the lateral adaptive preview strategy and longitudinal velocity planning for highly automated vehicle. *Vehicle System Dynamics*, *55*(8), 1143–1188. https://doi.org/10.1080/00423114.2017.1305114

Falcone, P., Borrelli, F., Asgari, J., Tseng, H. E., & Hrovat, D. (2007). Predictive active steering control for autonomous vehicle systems. *IEEE Transactions on Control Systems Technology*, *15*(3), 566–580. https://doi.org/10.1109/TCST.2007.894653

Funke, J., Brown, M., Erlien, S. M., & Gerdes, J. C. (2017). Collision Avoidance and Stabilization for Autonomous Vehicles in Emergency Scenarios. *IEEE Transactions on Control Systems Technology*, *25*(4), 1204–1216. https://doi.org/10.1109/TCST.2016.2599783

Gao, L., Beal, C., Fescenmyer, D., & Brennan, S. (2021). Analytical Longitudinal Speed Planning for CAVs with Previewed Road Geometry and Friction Constraints. *IEEE Conference on Intelligent Transportation Systems, Proceedings, ITSC*, *2021-Septe*, 1610–1615. https://doi.org/10.1109/ITSC48978.2021.9564602

Katriniok, A., Maschuw, J. P., Christen, F., Eckstein, L., & Abel, D. (2013). Optimal vehicle dynamics control for combined longitudinal and lateral autonomous vehicle guidance. *2013 European Control Conference, ECC 2013*, 974–979. https://doi.org/10.23919/ecc.2013.6669331

Litman, T. (2022). *Autonomous Vehicle Implementation Predictions: Implications for Transport Planning*.

Mattingley, J., & Boyd, S. (2012). CVXGEN: A code generator for embedded convex optimization. *Optimization and Engineering*, *13*(1), 1–27. https://doi.org/10.1007/s11081-011-9176-9

Ni, J., Hu, J., & Xiang, C. (2017). Envelope Control for Four-Wheel Independently Actuated Autonomous Ground Vehicle Through AFS/DYC Integrated Control. *IEEE Transactions on Vehicular Technology*, *66*(11), 9712–9726. https://doi.org/10.1109/TVT.2017.2723418

Pacejka, H. B. (2012). Tire and Vehicle Dynamics. In *Tire and Vehicle Dynamics*. https://doi.org/10.1016/b978-0-08-097016-5.00001-2

Panahandeh, G., Ek, E., & Mohammadiha, N. (2017). Road friction estimation for connected vehicles using supervised machine learning. *IEEE Intelligent Vehicles Symposium, Proceedings*, *Iv*, 1262–1267. https://doi.org/10.1109/IVS.2017.7995885

Yu, L., Zheng, S., Dai, Y., Abi, L., Liu, X., & Cheng, S. (2021). A feedback-feedforward steering controller designed for vehicle lane keeping in hard-braking manoeuvres on split-μ roads. *Vehicle System Dynamics*. https://doi.org/10.1080/00423114.2020.1869274